Title

Functional and structural characterization of the insertion region in the ligand binding domain of the vitamin D nuclear receptor

Journal

The FEBS Journal, 268(4)

ISSN

1742-464X

Authors

Rochel, Natachu
Tocchini-Valentini, Guiseppe
Egea, Pascal F
et al.

Publication Date

2001-02-01

DOI

10.1046/j.1432-1327.2001.01953.x

Peer reviewed

Eur. J. Biochem. **268**, 971–979 (2001) © FEBS 2001

Functional and structural characterization of the insertion region in the ligand binding domain of the vitamin D nuclear receptor

Natachu Rochel[1], Guiseppe Tocchini-Valentini[1], Pascal F. Egea[1], Kari Juntunen[2], Jean-Marie Garnier[1], Pirkko Vihko[2] and Dino Moras[1]

[1]*Laboratoire de Biologie et Génomique Structurale, UPR 9004, Institut de Génétique et de Biologie Moléculaire et Cellulaire, CNRS/INSERM/ULP, Illkirch Cedex, France;* [2]*Biocenter Oulu and WHO Collaborating Center for Research on Reproductive Health, University of Oulu, Finland*

Vitamin D nuclear receptor mediates the genomic actions of the active form of vitamin D, $1,25(OH)_2D_3$. This hormone is involved in calcium and phosphate metabolism and cell differentiation. Compared to other nuclear receptors, VDR presents a large insertion region at the N-terminal part of the ligand binding domain between helices H1 and H3, encoded by an additional exon. This region is poorly conserved in VDR in different species and is not well ordered as observed by secondary structure prediction. We engineered a VDR ligand binding domain mutant by removing this insertion region. Here we report its biochemical and biophysical characterization. The mutant protein exhibits the same ligand binding, dimerization with retinoid X receptor and transactivation properties as the wild-type VDR, suggesting that the insertion region does not affect these main functions. Solution studies by small angle X-ray scattering shows that the conformation in solution of the VDR mutant is similar to that observed in the crystal and that the insertion region in the VDR wild-type is not well ordered.

Keywords: nuclear receptor; VDR LBD; ligand binding; conformation; transactivation.

Steroids, retinoids, thyroid hormone and vitamin D_3 mediate their pleitoric effects through ligand-dependent transcription factors, the nuclear receptors [1,2]. These receptors control cell growth and differentiation, homeostasis, development and other physiological processes by modulating target genes. Members of the nuclear receptors superfamily exhibit the same modular structure with a variable N-terminal domain (A/B region), a conserved DNA binding domain (DBD, C region), a flexible hinge region (D region) and a moderately conserved ligand binding domain (LBD, E/F region). The A/B region is the most divergent among the nuclear receptors and contains a ligand independent activation function AF-1. The LBD contains a dimerization interface and a ligand-dependent transcriptional activation domain AF-2. The crystallographic structures of ligand binding domains of several liganded and unliganded nuclear receptors (reviewed in [3,4]) have shown that they share a common fold with 11–13 α helices 'sandwiched' in three layers. Ligand binding induces a conformational change in the orientation of the AF-2 core motif that allows the interaction with coactivators that facilitate the interaction between the nuclear receptor and the basal transcription machinery [3]. Several coactivators [5–7] have been identified as the SRC coactivators family, the DRIP/TRAP coactivators or cointegrators (CBP/P300). They all present a LXXLL motif, a requirement for the interaction with the AF-2 domain of nuclear receptors. Efficient transcriptional regulation is achieved through the interaction of nuclear receptors with coregulator and the recruitment to the promoter of diverse functional domains responsible of acetylation, deacetylation, phophorylation, ligation or proteolysis [6].

The vitamin D nuclear receptor (VDR) mediates the genomic actions upon binding to the active form of vitamin D, $1,25(OH)_2D_3$. VDR heterodimerizes with retinoid X receptor (RXR) and binds with high affinity to specific vitamin D-responsive element (VDRE), at 5′ flanking region of target genes in order to regulate transcription of the upstream gene [8]. $1,25(OH)_2D_3$ regulates the calcium and phosphate metabolism (stimulation of bone growth and mineralization and regulation of the calcium and phosphate intestinal absorption), induces potent cell differentiation activity and has immunosuppressive effects [9,10]. Furthermore it inhibits the growth of a number of primary and cultured tumor cell types (breast, prostate, colon, and lymphomas). Therapeutic or potential therapeutic applications of vitamin D metabolites are treatments for renal osteodystrophy, osteoporosis, psoriasis, cancer, autoimmune diseases or prevention of graft rejection. These applications are limited by the side-effects of the natural ligand (hypercalcemia and

Correspondence to D. Moras, Laboratoire de Biologie et Génomique Structurale, UPR 9004, Institut de Génétique et de Biologie Moléculaire et Cellulaire, CNRS/INSERM/ULP, 1 rue Laurent Fries, 67404 Illkirch Cedex, France. Fax: + 33 3 88 65 32 76, moras@igbmc.u-strasbg.fr

Abbreviations: DBD, DNA binding domain; LBD, ligand binding domain; SAXS, small angle X-ray scattering; RAR, retinoic acid receptor; RXR, retinoid X receptor; VDR, vitamin D receptor; VDRwt, VDR LBD wild-type; VDRmt, VDR LBD mutant; $1,25(OH)_2D_3$, 1α,25-dihydroxyvitamin D_3; VDRE, vitamin D response element.

(Received 6 October 2000, accepted 7 December 2000)

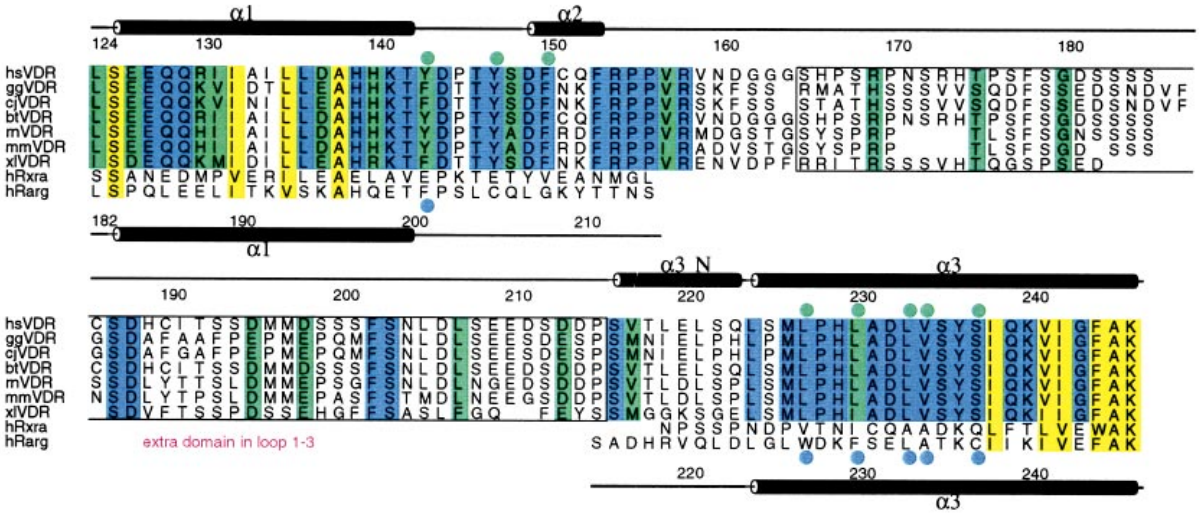

Fig. 1. Structure based VDR sequence alignment in the H1-H3 region. VDR sequences of different species: hs, *Homo sapiens* (human); gg, *Gallus gallus* (chicken); *cj*, *Coturnic japonica* (japanese quail); bt, *Bos taurus* (bovine); mm, *musculus* (mouse); xl, *Xenopus laevi* (african clawed frog); rn, *Ratus norvegicus* (rat); together with the sequences of the human RXRα (hRXRα) and human RARγ (hRARγ). The secondary structures of the hVDR and the hRARγ molecules as seen in the crystal structures are shown at the top and bottom of the alignment, respectively, together with their sequence numbering. The residues lining the pocket are indicated as green and blue dots. The yellow box corresponds to the conserved residues between the VDR and hRXRα and hRARγ.

soft tissue calcification). A large number of vitamin D analogs have been synthesized in order to separate the anti-proliferative and calcemic activities [9]. Several analogs have been shown to have high anti-proliferative properties with less calcemic effects compared to vitamin D, but the underlying molecular mechanism is still not understood.

A typical feature of VDR [11] is the presence of a large insertion domain at the N-terminal part of the LBD (Fig. 1) in the peptide connecting helices H1 and H3. The length of this connecting region varies between 72 and 81 residues in the VDR family compared to 15–25 residues for the other nuclear receptors. This insertion domain, for which no biological function has been found until now, is poorly conserved between the VDR species (9% identity between amino acids 157–215 of hVDR) and is encoded by an additional exon in the VDR chromosomal gene [10]. One mutation associated with the genetic disease, vitamin-D-resistant rickets, has been found in this region (Cys190→Trp) with no effect on ligand binding [10]. A phosphorylation site has been identified at Ser208 [12]. Recently we have engineered a VDR LBD without this extra domain and have solved the crystallographic structure of this VDR LBD mutant (VDRmt) bound to its natural ligand $1,25(OH)_2D_3$ [13]. The overall fold of this protein is similar to the agonist fold of other nuclear receptors.

In this paper we describe the cloning, purification and the characterization of the properties (binding, trans-activation, dimerization) of this VDR LBD mutant by biochemical and biophysical methods and we compare them with those of the wild-type VDR LBD (VDRwt). We present also a small angle X-ray scattering study (SAXS) of the VDRwt and VDRmt complexed with $1,25(OH)_2D_3$. The scattering curve of the VDRmt calculated from the atomic structure and the comparison with the experimental scattering curves of the VDRwt and VDRmt provide structural information about the insertion domain.

EXPERIMENTAL PROCEDURES

Plasmid construction

The chimeras Gal4–VDR (118–427) and Gal4–VDR mutant (118–427, Δ165–215) were constructed by PCR using the appropriate oligonucleotides with restriction sites (*Xho*I/*Bam*HI) and the pSG5 VDR plasmid (1–427) as template and cloned into the vector PXJ440 encoding the DBD of the yeast activator Gal4 (1–147). The pSG5 VDR (1–427) was used to construct the pSG5 VDR mutant (1–427, Δ165–215). For overexpression in *Escherichia coli*, VDR (118–427) and VDR mutant (118–427, Δ165–215) were subcloned into the *Nde*I/*Bam*HI sites of pET15b. All constructs were verified by automated DNA sequencing.

Expression and purification

Human VDRwt (118–427) and VDRmt (118–427, Δ165–215) were overproduced as hexahisdines-tagged proteins in *E. coli* BL21 (DE3) (Novagen). A 200-mL Luria–Bertani preculture containing 200 μg ampicillin per mL was grown overnight at 37 °C and 25-mL aliquots of the preculture were used to inoculate a 1-L Luria–Bertani culture containing 200 μg ampicillin per mL. Cells were grown at 37 °C to D_{600} = 0.6, and were allowed to grow 6 h at 20 °C after induction by addition of 1 mM isopropyl thio-β-D-galactoside. Cells were harvested by centrifugation and the pellets were frozen and kept at −80 °C. The cell pellet from 1 L of culture was resuspended in 25 mL buffer containing 5 mM imidazole, 20 mM Tris/HCl pH 8.0,

250 mM NaCl, 5% glycerol, 1 mM protein inhibitor cocktail (PIC) and 1 mM protein inhibitor cocktail (PIC) 2-mercaptoethanol. The cells were lysed by sonication. The crude extract was loaded on an immobilized metal affinity column (Talon, Clontech) and eluted with imidazole. The fractions of interest were pooled and digested with bovine thrombin (1 unit per mg of protein) overnight at 4 °C in presence of 5 mM $CaCl_2$ to remove the histidine tag. The protein was incubated with an excess of $1,25(OH)_2D_3$ and loaded on a gel-filtration Superdex 75 16/60 (Pharmacia) equilibrated in 10 mM Tris/HCl pH 7.0, 100 mM NaCl, 10 mM dithiothreitol. The protein purity was analyzed by SDS/PAGE on a 12.5% polyacrylamide gel and native PAGE on an 8–25% gradient polyacrylamide gel and Coomassie blue staining. Protein concentration was determined by Bradford using BSA as standard and by UV spectrophotometry considering the absorption coefficients ($M^{-1}\cdot cm^{-1}$) $\varepsilon = 16\,410$ and 16 290 for VDRwt and VDRmt, respectively, at $\lambda = 280$ nm.

Analytical gel filtrations

Analytical gel filtrations were performed on a Superdex 200-HR 10/30 column (Pharmacia) with a flow rate of 0.5 $mL\cdot min^{-1}$ and an injection volume of 0.5 mL. The column was calibrated with proteins of known molecular masses. The buffer was 10 mM Tris pH 8.0, 250 mM NaCl, 1 mM EDTA, 5 mM dithiothreitol, 1 mM Chaps and 0.05 mM *n*-dodecyl α-D-maltoside and the concentration of the complex was 1.8 $mg\cdot mL^{-1}$. VDRwt and VDRmt complexed to $1,25(OH)_2D_3$ eluted as monomeric species. The top of the gel-filtration peak was used for scattering measurements without further concentration to avoid aggregation problems.

Mass spectra

For electrospray ionization mass spectra, proteins were concentrated on Centricon 30 to 4 $mg\cdot mL^{-1}$ and dialyzed extensively against ammonium acetate 50 mM pH 7.0.

Ligand binding

Ligand binding assays were performed on crude extracts of *E. coli* BL21 (DE3) expressing VDRwt or VDRmt. For Scatchard analyses, the crude extracts were diluted 1000 times and incubated with increasing amounts of [26,27-^{3}H]$1,25(OH)_2D_3$ (Amersham) in 20 mM Tris, 250 mM NaCl, 5 mM dithiothreitol, 10% glycerol for 16 h at 4 °C. After incubation, 25 μL of dextran/charcoal (1.5%) were added to 25 μL of the protein mixture. After 5 min the tubes were centrifuged at 14 000 ***g*** for 5 min. The concentrations of the bound ligand (B) were determined by liquid scintillation counting on supernatant. Total ligand concentrations were measured by liquid scintillation counting 15 μL of the protein mixture before adding dextran/charcoal. U represents the unbound ligand. Each point represents an average of three values. Data were analyzed by nonlinear least square method as described previously [14] for a model of one specific binding site and nonspecific binding sites. The competition assays with the analogs MC903 [1α,(24*S*)-$(OH)_2$-22-ene-26,27-cyclopropyl vitamin D_3), EB1089 (1α,25-dihydroxy-22,24-diene-24,26,27-tri-homo-vitamin D_3) and KH1060 (20-epi-22-oxa-24a,26,27a-tri-homo-1α,25-dihydroxy vitamin D_3) were performed as described previously [15]. The diluted crude extracts were incubated with 1 nM of [^{3}H-26,27] $1,25(OH)_2D_3$ and increasing concentrations of $1,25(OH)_2D_3$ analogs for 12–16 h at 4 °C. The bound and free ligands were separated by dextran/charcoal. Non-specific binding was measured in the presence of 250-fold excess of $1,25(OH)_2D_3$. The concentrations of the radio-inert vitamin D stock solution was measured by absorbance at 265 nm ($\varepsilon = 18\,200\ M^{-1}\cdot cm^{-1}$). The experiments were performed twice in triplicate.

Dimerization with RXR

The his-tagged VDRmt (pET28a) and nontagged hRXRα LBD (pET3a) were coexpressed and purified in three steps. The cell pellets were lysed by sonication. The heterodimer was purified on metal affinity column (Talon, Clontech) using imidazole elution, followed by gel-filtration on a Superdex S75-HR 26/60 (Pharmacia). The tagged monomer of VDRmt in excess was easily removed in this step. Fractions containing the heterodimer were pooled together and treated with bovine thrombin (1 unit per mg of protein) overnight at 4 °C in presence of 5 mM $CaCl_2$ to remove the histidine tag. The final step is the purification of the dimer on an analytical gel filtration on a Superdex S200-HR 10/30 (Pharmacia). Ligands were added in excess throughout the first two steps.

Analytical centrifugation

Sedimentation equilibrium was performed on the LBD heterodimer VDRmt/hRXRα complexed to $1,25(OH)_2D_3$ and 9-*cis* retinoic acid on a Beckman XLA analytical ultracentrifuge (Institut de Pharmacologie et de Biologie Structurale, Toulouse, France). The complex was prepared in a buffer containing 20 mM Tris pH 8.0, 1 mM EDTA and 250 mM KCl. Experiments were carried out at 20 °C in 1.2-cm path length double-sector cells and run at 12 000 r.p.m. After 12 h centrifugation, scans were compared at 2 h intervals to ensure that the equilibrium was reached. Data were analyzed by single or multifit analysis programs supplied by Beckman as described previously [16]. Different models of association were used to analyze the data.

Cell culture, transfection and transactivation assays

COS cells (SV40-transformed African Green monkey kidney) were maintained in Dulbecco's modified Eagle's medium supplemented with 10% dextran-coated charcoal-stripped fetal bovine serum. Cells were plated in 100-mm culture dishes and transfected using the calcium phosphate coprecipitation. Forty-eight hours following transfection, cells were harvested by three freeze-thaw cycles. Transactivation assays were performed on two systems. Transfections were carried out as described previously [17] with for the first system, precipitates containing 250 ng of receptor expression vectors PXJ440 VDRwt or VDRmt, 2 μg of reporter gene 5 × 17m-TATA-CAT (chloramphenicol acetyltransferase), 2 μg of an internal control recombinant expressing β-galatosidase pCH110lacZ (Pharmacia) made up to 20 μg with carrier DNA. For the

second system, 500 ng of pSG5 VDR (1–427) or VDR mutant (1–427, Δ165–215) were cotransfected with 2 μg of reporter gene rat osteopontin VDRE-tk (thimidine kinase)–Luc (luciferase), 2 μg of pCH110lacZ made up to 20 μg with carrier DNA. Cells were treated with 100 nM $1,25(OH)_2D_3$ or ethanol vehicle. β-Galactosidase activity was determined by colorimetric assay with *o*-nitrophenyl-β-D-galactopyranoside (Sigma) and normalized for transfection efficiency against β-galactosidase enzyme (Sigma) standards. Chloramphenicol acetyltransferase activity was quantified by ELISA (Boehringer Mannheim) according to the manufacturer's instructions. Luciferase activity was measured with luciferase assay reagent (Promega) in a luminometer. Luciferase and chloramphenicol acetyltransferase activities were both standardized using galactosidase activities. Results are given as a percentage of maximal VDR wild-type in the presence of 100 nM $1,25(OH)_2D_3$. Experiments were performed twice in triplicate.

Small angle X-ray scattering (SAXS)

The buffer for X-ray scattering measurements was 10 mM Tris/HCl pH 8.0, 250 mM NaCl, 10 mM dithiothreitol, 1 mM EDTA, 0.1 mM di-isopropyl fluorophosphate, 1 mM Chaps and 0.05 mM *n*-dodecyl α-D-maltoside. The concentrations of the VDR wild-type were 3.8 and 4.9 $mg{\cdot}mL^{-1}$ and of the VDR mutant 2.0 $mg{\cdot}mL^{-1}$. SAXS measurements were recorded at 5 °C on the D24 small angle scattering instrument using synchrotron radiation at LURE-DCI, Orsay, France [18]. The X-ray wavelength was 1.488 Å and the detector distance was 1573 mm. An assymetric experimental setup was used in order to simultaneously record data in small and high Q regions. The effective Q range extended from 0.01 to 0.48 $Å^{-1}$ but was reduced from 0.01 to 0.3 $Å^{-1}$. Nine frames of 200 s each were recorded for each sample. Each frame was individually visualized to check the absence of denaturation or aggregation during data collection. The scattering intensity of a reference sample of carbon black recorded before and after each sample was used to normalize all data to the transmitted intensity. The scattering of the buffer was subtracted before analysis. The data acquisition was performed with the program OTOKO.

Scattering curves calculation

X-ray scattering curves were computed from crystallographic coordinates of the VDR mutant [13] using the program CRYSOL [19,20], which takes into account the hydration layer surrounding the protein surface and can be fitted against experimental curves. In this program, a particle envelope is represented by an angular function connecting the center of mass with the most distant atom along each direction. The hydration shell is approximated by a 0.3-nm-thick concentric border layer placed 0.2 nm outside the envelope to model the density profile of the first shell. The electron density contrast of this layer and the excluded volume of the particle are adjustable parameters when fitting the experimental scattering curves.

Analysis of reduced X-ray data

The scattering intensity $I(Q)$ from a dilute monodisperse solution is an isotropic function proportional to the scattering from a single particle averaged over all orientations, and the experimental curves are obtained by subtracting the solvent contribution. Recording of the scattering intensities allows determination of the radius of gyration R_G that is a measure of structural elongation if the internal inhomogeneity of scattering densities within the protein can be neglected. Analysis of the $I(Q)$ curves at small Q in Guinier plots give the radius of gyration R_G and the forward scattering at zero scattering angle $I(0)$ [21]:

$$\ln I(Q) = \ln I(0) - R_G^2 Q^2/3 \text{ with } Q = 4\pi \sin \theta/\lambda$$

where Q is the scattering vector for a scattering angle of 2θ and a wavelength λ. The expression is valid in a QR_G range up to 1.5. The relative value of $I(0)/c$ with c the sample concentration, gives the apparent molecular mass m of the particle in solution. m is calculated by using a lysozyme solution at 6 $mg{\cdot}mL^{-1}$ in 100 mM NaCl, 50 mM sodium acetate pH 4.6, as a molecular mass standard reference. If the structure is sufficiently elongated, the averaged radius of gyration of the cross-sectional structure R_{XS} and the averaged cross-sectional intensity at zero angle $[I(Q)\,Q]_{Q\to 0}$ are obtained from [22]:

$$\ln [I(Q)Q] = \ln [I(Q)\,Q]_{Q\to 0} - R_{XS}^2 Q^2/2$$

The R_G and R_{XS} analyses lead to estimates of the length of the longest axis L of the particle in solution with $L = [12(R_G^2 R_{XS}^2)]\}^{1/2}$ [22]. The QR_{XS} ranges for VDRwt and VDRmt were $0.8 \leq QR_{XS} \leq 2.0$ and $0.7 \leq QR_{XS} \leq 1.8$, respectively.

Indirect transformation of the full scattering data $I(Q)$ in the reciprocal space into that in real space provides $P(r)$, the interatomic distances radial distribution function. The distance distribution function $P(r)$ corresponds to the distribution of distances r between any two volume elements within one particle and is obtained by indirect Fourier transformation algorithms that suppress truncation artifacts due to the limited reciprocal space of the scattering. In this study $P(r)$ functions were calculated using the program GNOM [23]. This function offers an alternative calculation of $I(0)$, its zeroth moment, and of R_G, its second moment, and gives the maximum dimension of the molecule D_{max}.

$$P(r) = \frac{1}{2\pi^2}\int_0^\infty I(Q)Qr \sin (Qr)\mathrm{d}Q$$

The criteria to evaluate correctly the $P(r)$ distribution function [24] were satisfied in this study. D_{max} between 55 and 90 Å correspond to $Q_{min} = 0.057$ $Å^{-1}$ and 0.034 $Å^{-1}$. D_{max} was determined from the value of r when $P(r)$ became zero at large r. The X-ray $I(Q)$ curves contained 255 points ($0.01 < Q < 0.3$ $Å^{-1}$). D_{max} was varied in 1 Å steps between 50 and 100 Å to test the stability of the $P(r)$ transformation.

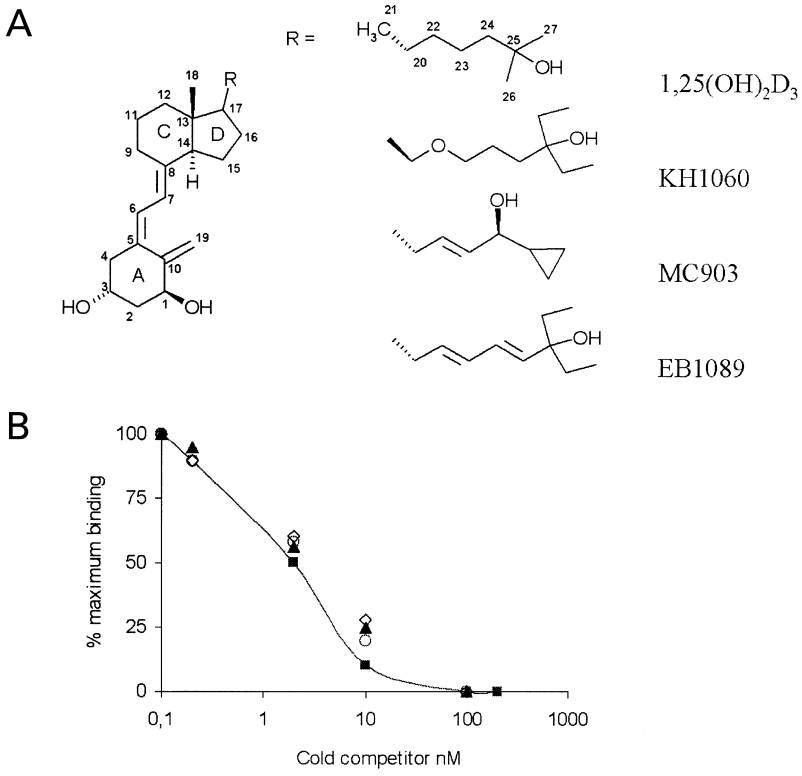

Fig. 2. Chemical structures of $1,25(OH)_2D_3$ analogs (a) and competition binding analysis of VDRmt (b). ■, $1,25(OH)_2D_3$; ○, MC903; ▲, EB1089; ◇, KH1060. Values shown are means from two experiments in triplicate. The data are represented as percent of specific binding.

Fig. 3. Crystallographic structure of the VDRmt bound to $1,25(OH)_2D_3$ [13]. The residues surrounding the deletion are shown in orange.

RESULTS AND DISCUSSION

Biological characterization of the VDR LBD mutant

The VDR LBD wild-type is poorly soluble and accumulates in inclusion bodies. In previous reports on the expression and purification of *E. coli* VDR, the protein was solubilized by renaturation of inclusion bodies [25,26] or by expression of the VDR LBD fused to the glutathione *S*-transferase [27] or the maltose binding protein [28]. Lower amounts of the protein has also been purified from yeast [29] or insect cells using baculovirus [30,31]. The insertion region is not well ordered according to secondary structure prediction and presents only few short β strands. Furthermore, this region is sensible to proteolysis with a trypsin cleavage site after Arg174 of hVDR [32]. The removal of the insertion domain in the VDR mutant stabilizes the protein by lowering the number of conformations adopted by the insertion domain of VDRwt. Two milligrams of soluble purified VDR LBD mutant protein, lacking the residues 165–215 of hVDR (Fig. 1) and leaving 30 residues to connect helices H1 to H3, can be obtained from 1 L of culture. Thus the deletion of the insertion domain increases the solubility of the protein. The mutant behaves as a monomeric species on gel filtration and migrates as a single band on native PAGE. The experimental masses measured by mass spectrometry for VDRwt and VDRmt bound to $1,25(OH)_2D_3$ were 35 652 ± 2 Da and 30 206 ± 2 Da, respectively; the theoretical calculated values are 35 633 Da and 30 185 Da, respectively.

We have previously reported the dissociation constants K_d of vitamin D for the VDRwt ($K_d = 0.55$ nM) and VDRmt ($K_d = 0.37$ nM) [13] and have shown that there is

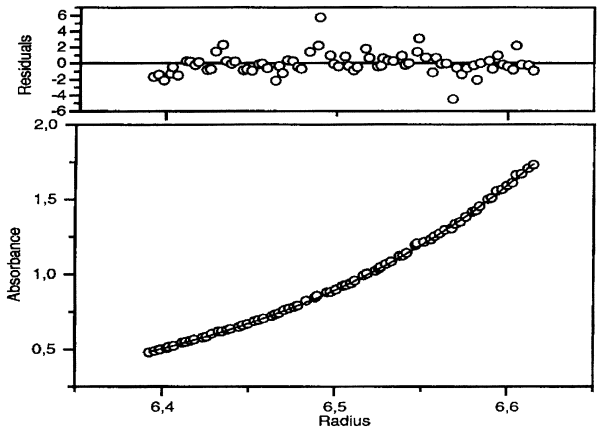

Fig. 4. Sedimentation equilibrium analysis of VDRmt/RXR complex. The absorbance is plotted as a function of *r*. The best fitting curve is shown on the graph for a model with a single ideal species. The distribution of the reduced residuals are shown on the top of the figure.

no significant difference between values for the two proteins. These values agreed well with those previously obtained for recombinant VDR from *E. coli*, yeast and insect cells [25–31]. To compare the relative binding affinities for VDRmt of $1,25(OH)_2D_3$ and several $1,25(OH)_2D_3$ agonists analogs, MC903, EB1089 and the 20-epi KH1060 (Fig. 2a), ligand-binding competition experiments were performed with [^{3}H]$1,25(OH)_2D_3$ and unlabeled analogs (Fig. 2b). All these compounds are potent anti-proliferative drugs. $1,25(OH)_2D_3$ exhibits the highest affinity for VDRmt and the relative affinities of the compounds MC903, EB1089 and the 20-epi analog KH1060 for VDRmt, at 2 nM compared to 100% for $1,25(OH)_2D_3$ are 86, 83 and 90%, respectively. Similar results on the relative affinities of these analogs for VDRmt were obtained by native electrospray ionization mass spectroscopy (data not shown). Therefore, VDRmt binds these analogs with similar affinity compared to the VDRwt [9]. In the crystal structure of VDRmt bound to $1,25(OH)_2D_3$ (Fig. 3), the location of the truncated insertion domain shown in orange, is distant from the ligand and is unlikely to affect the binding of the ligand.

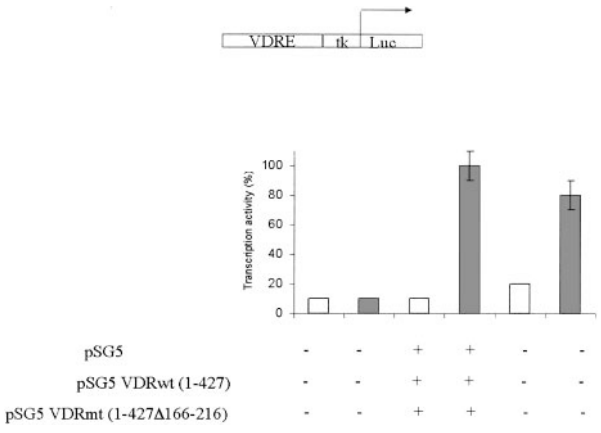

Fig. 5. Relative luciferase activity of the hVDRwt full length (1–427) and of the hVDRmt (1–427, Δ166-216). The structure of the reporter construct is shown schematically on the top. Luciferase activities are expressed relative to the VDRwt + $1,25(OH)_2D_3$ induced activity (100%). pSG is the parent plasmid.

VDR modulates gene activity by forming heterodimer complexes with RXR isoforms and specific DNA sequences, and they interact with elements of the transcriptional machinery in the presence of their endogenous ligands, $1,25(OH)_2D_3$ and 9-*cis* retinoic acid. It was therefore important to investigate if this VDR mutant was able to form an heterodimer with RXR. The purified VDRmt/RXRα LBDs complexed to $1,25(OH)_2D_3$ and 9-*cis* retinoic acid is a stable species and the two partners are able to bind their ligands as seen by native electrospray ionization mass spectroscopy (data not shown). The stability of this complex was measured by analytical ultracentrifugation. Only one species of 53 000 ± 600 (± 2 σ) Da could be detected by equilibrium sedimentation corresponding to the theoretical heterodimer (Fig. 4). Attempts to fit the data using a system with an heterodimer in equilibrium with free monomeric subunits resulted in bad statistical fits, thus pointing out the stability and homogeneity of the heterodimeric species. Several biophysical studies using surface plasmon resonance [33], fluorescence anisotropy [34] and electrospray mass spectra [35], on full length VDR/RXRα/DNA complexes have shown that $1,25(OH)_2D_3$ favors heterodimerization while 9-*cis* retinoic acid reduces it. But maximal heterodimerization was observed in the presence of both ligands [35].

To study the ability of VDRmt fused to Gal4–DBD to activate transcription in a $1,25(OH)_2D_3$-dependent manner, COS cells were transiently transfected with a Gal4 responsive reporter. Transfected cells were treated with either vehicle alone or $1,25(OH)_2D_3$ and assayed for chloramphenicol acetyltransferase activity. $1,25(OH)_2D_3$-dependent enhancement of chloramphenicol acetyltransferase activity upon expression of VDR wild-type LBD fused to the DBD of Gal4, was observed. The expression of VDRmt in transfected cells was similar to that of the wild-type and the relative transactivation ability of the VDRmt was 80% of the activation of the VDRwt in the presence of ligand (100%). The same results were obtained with the full length VDR cotransfected with a luciferase reporter plasmid containing the osteopontin gene VDRE under the control of the thymidine kinase promoter (Fig. 5). The transactivation of VDR is mediated by the ligand-dependent function present in the LBD. These results indicate that the insertion region of VDR is not involved in the activation function of this nuclear receptor. Thus VDRmt behaves like the VDRwt in ligand-binding, heterodimerization with RXRα and transactivation.

Solution studies of the VDR mutant and VDR wild-type

To obtain structural information on the insertion domain of the VDRwt, we have carried out SAXS, a powerful technique providing low resolution information in solution [36,37]. All structural information is contained in the scattering intensity I(Q,t) as a function of time t and of scattering angle Q. As there are no preferable orientations among the particles, the scattering function is time and space averaged. In the small Q region, the scattering function can be approximated by the Guinier's formulae allowing determination of the radius of gyration, R_G, and

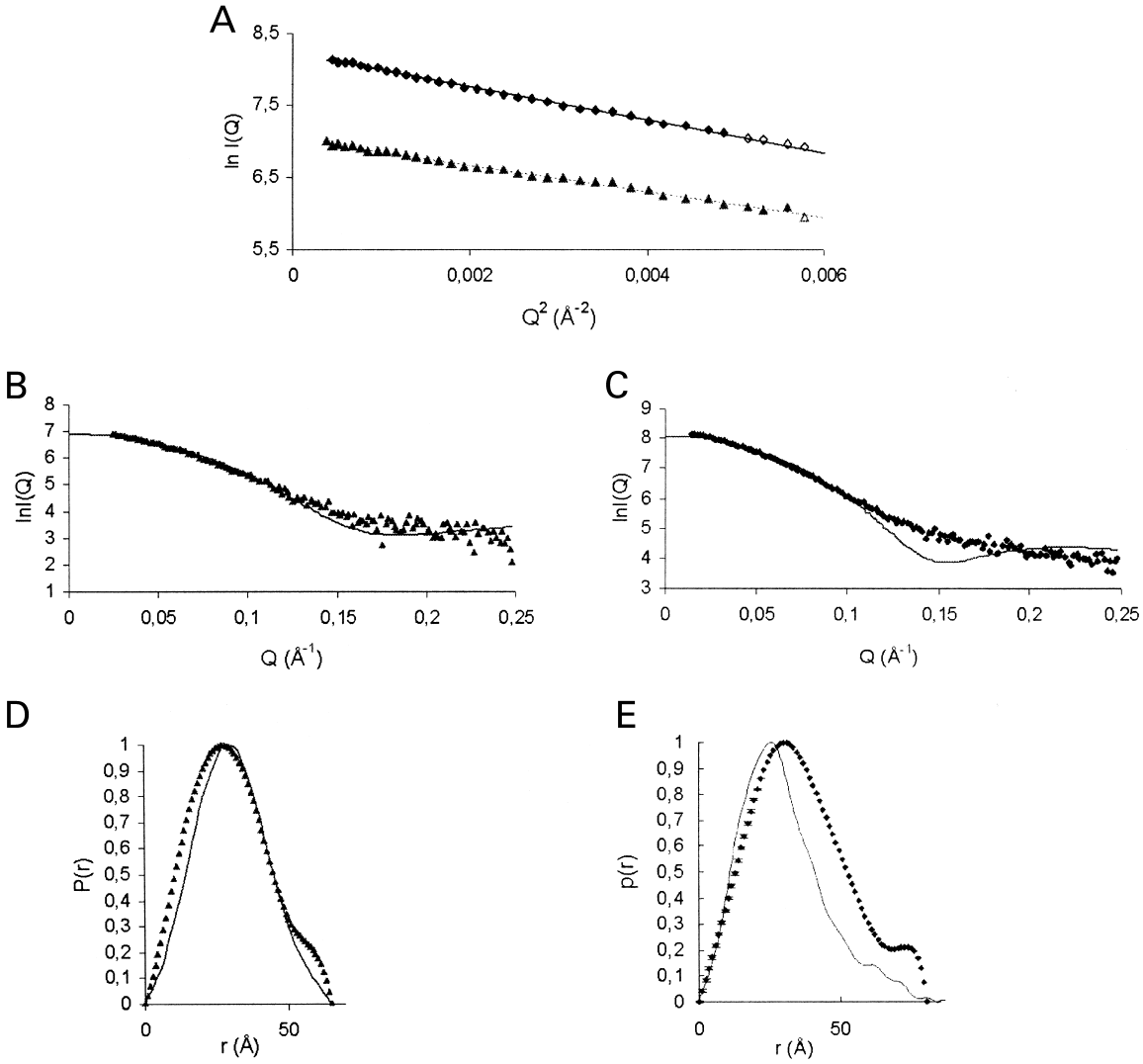

Fig. 6. Solution scattering analysis of VDRwt (u) and VDRmt (▲) bound to 1,25(OH)$_2$D$_3$. (a) Guinier analysis. Filled symbols are the data points used to determine the R_G values. The QR_G ranges for VDRwt and VDRmt are $0.55 \leq QR_G \leq 1.8$ and $0.46 \leq QR_G \leq 1.7$, respectively. (b) and (c) X-ray scattering curves of VDRmt and VDRwt, respectively. Experimental curves calculated with CRYSOL [19,20] were fitted against calculated curve (continuous line) from the crystallographic structure of VDRmt holo. (d) and (e) Distance distribution function $P(r)$ of VDRmt and VDRwt, respectively. The $P(r)$ function calculated with the program GNOM [23] from the theoretical scattering curve of VDRmt crystal structure is shown as a continuous line.

the forward scattering at zero scattering angle, I (0), and providing information on the molecular compactness and the molecular mass of the particle. In the high Q region, I(Q,t) reflects the fluctuation of the scattering density distribution within the particle and provides information of the inner structure rather than the global shape. The direct Fourier transformation of I(Q,t) called $P(r)$, the interatomic distances radial distribution function, gives the scattering elements density distribution of the particle and allows the determination of the longest distance, D_{max}, in the molecule. We have already reported a small angle neutron scattering study of the VDRwt in its non-ligand-bound and ligand-bound forms and have shown that the ligand-bound form is more compact, in agreement with the conformational change in the orientation of the AF-2 motif [31].

Linear Guinier plots (Fig. 6a) were obtained for VDRwt and VDRmt in satisfactory QR_G ranges. No aggregation was detected at the concentrations used. Thus, VDRwt and VDRmt appear perfectly homogenous and monodisperse. Each R_G measurement was carried out on two different, independently prepared samples. Apparent mass calculations (Table 1) were performed from the $I(0)$ values and are in agreement with the expected mass for monomeric species. No equilibrium between different species of higher order were detected, in agreement with the monomer observed in the crystal structure of VDRmt bound to 1,25(OH)$_2$D$_3$. The radii of gyration (Table 1) of VDRwt and VDRmt complexed to 1,25(OH)$_2$D$_3$ are 26.2 and 23.4 Å, respectively. The difference of 2.8 Å observed between the radii of gyration of the two proteins corresponds to an increase in volume of 35%

Table 1. Summary of solution scattering data for VDRwt and VDRmt complexes with $1,25(OH)_2D_3$.

	m [$I(0)/c$] (kDa)	R_G (Å)	R_{XS} (Å)	D_{max} (Å)
VDRwt	37	26.2 ± 0.1 (Guinier) 27.2 ± 0.1 [$P(r)$]	13.9	80 (Guinier) 80 [$P(r)$]
VDRmt	29	23.4 ± 0.1 (Guinier) 23.8 ± 0.1 [$P(r)$]	12.8	68 (Guinier) 65 [$P(r)$]
Crystal structure		22.6		

for a spherical object. A similar difference (2.2 Å) has been observed by small angle neutron scattering (data not shown) between VDRwt and VDRmt. This difference is rather large and suggests a disordered insertion domain.

Experimental scattering curves for VDRwt and VDRmt (Fig. 6b,c) were fitted against the theoretical curve calculated from the crystal structure of VDRmt bound to $1,25(OH)_2D_3$, using the program CRYSOL [19,20]. The experimental scattering curve of the VDRmt fits well with the curve calculated from the crystallographic structure, indicating that the conformation in solution for the VDRmt is similar to that observed in the crystal. The value of the radius of gyration of VDRmt from the crystallographic structure is 22.6 Å (atom-excluded volume + shell), which is close to the experimental value.

The interatomic distances radial distribution $P(r)$ were calculated from SAXS data for VDRwt and VDRmt. The experimental curve of VDRmt fits well with the curve calculated from the crystal structure (Fig. 6d) confirming the agreement of the solution and crystal structures of VDRmt. Due to the low concentration of the two proteins used in this study, only estimates of D_{max} were obtained (Table 1). The difference of 15 Å between the D_{max} values of VDRmt and VDRwt is rather large for an additional domain of 50 residues, suggesting that this insertion domain is not well ordered and may adopt several conformations in solution. The R_G values calculated from $P(r)$ functions are in agreement with those calculated from Guinier analysis.

As seen in the crystal structure of VDRmt (Fig. 3), the overall shape is ellipsoidal with its longest axis colinear to a N- to C-terminal axis including helix H12. D_{max} changes show that the additional insertion region may be positioned along this axis, keeping in mind that small angle scattering data are time and space averaged, suggesting that the insertion region is likely to adopt several conformations in solution.

The present study shows that the insertion domain between helices H1 and H3, VDR specific, is not involved in the main biological functions of VDR: ligand binding, dimerization with RXR and ligand-dependent transactivation. The structural studies by small angle X-ray scattering experiments show that the conformation in solution of VDRmt bound to $1,25(OH)_2D_3$ is similar to the conformation in the crystal and confirm that the insertion domain is not well ordered in solution. We propose a model of VDRwt with the insertion domain highly mobile with the rest of the LBD structured similarly to that of VDRmt. Note that the proposed nuclear localization sequence motif (154–158) is still present in our VDR mutant. The clear biological role of this domain is still not clear; this insertion (154–173) appears to play a role in the transport of VDR into the nucleus [38].

ACKNOWLEDGEMENTS

We are grateful to A. Steinmeyer (Schering AG) for a generous gift of $1,25(OH)_2D_3$ and of the synthetic analogs. We acknowledge P. Vachette (Beam D24, Lure, France) for assistance with the SAXS experiments. We thank N. Potier and A. Van Dorsselaer for mass spectroscopy experiments. We are grateful to C. Birck and J. P. Samama for the ultracentrifugation experiments. We also thank Y. G. Gangloff, L. Carré, M. Gangloff and J. Fagart for discussion for the transactivation and binding experiments. We acknowleledge J. M. Wurtz for careful reading of the manuscript and we thank the staff of the cell culture, oligonucleotides and DNA sequencing facilities. This work was supported by grants from the CNRS, the INSERM, the Hôpital Universitaire de Strasbourg, the Ministère de la Recherche et de la Technologie, the Association pour la Recherche contre le Cancer, the Ligue Nationale contre le cancer, the Academy of Finland and the Sigrid Juselius Foundation.

REFERENCES

1. Mangelsdorf, D.J., Thummel, C., Beato, M., Herrlich, P., Schütz, G., Umesono, K., Blumberg, B., Kastner, P., Mark, M., Chambon, P. & Evans, R.M. (1995) The nuclear receptor superfamily: the second decade. *Cell* **83**, 835–839.
2. Gronemeyer, H. & Laudet, V. (1995) Nuclear Receptor. In *Protein Profile: Transcription Factors 3.* (Sheterline, P, ed.), pp. 1173–1181. Academic Press, Liverpool, UK.
3. Moras, D. & Gronemeyer, H. (1998) The nuclear receptor ligand-binding domain: structure and function. *Curr. Opin. Cell Biol.* **10**, 384–391.
4. Egea, P.F., Klaholz, B.P. & Moras, D. (2000) Ligand–protein interactions in nuclear receptors of hormones. *FEBS Lett.* **476**, 62–67.
5. Robyr, D., Wolfe, A.P. & Wahli, W. (2000) Nuclear hormone receptor coregulators in action: diversity for shared tasks. *Mol. Endocrinol.* **14**, 329–347.
6. McKenna, N.J., Lanz, R.B. & O'Malley, B.W. (1999) Nuclear receptor coregulators: cellular and molecular biology. *Endocrinol. Rev.* **20**, 321–344.
7. Rachez, C. & Freedman, L.P. (2000) Mechanisms of gene regulation by vitamin D3 receptor: a network of coactivator interactions. *Gene* **246**, 9–21.
8. DeLuca, H.F. & Zierold, C. (1998) Mechanisms and functions of vitamin D. *Nutr. Rev.* **56**, 54–75.
9. Bouillon, R., Okamura, W.H. & Norman, A.W. (1995) Structure–function relationships in the vitamin D endocrine system. *Endocrinol. Rev.* **16**, 200–257.

10. Malloy, P.J., Pike, J.W. & Feldman, D. (1999) The vitamin D receptor and the syndrome of hereditary 1,25-dihydroxyvitamin D-resistant rickets. *Endocrinol. Rev.* **20**, 156–188.
11. Baker, A.R., McDonnell, D.P., Hughes, M., Crisp, T.M., Mangelsdorf, D.J., Haussler, M.R., Pike, J.W., Shine, J. & O'Malley, B.W. (1988) Cloning and expression of full-length cDNA encoding human vitamin D receptor. *Proc. Natl Acad. Sci. USA* **85**, 3249–3258.
12. Jurutka, P.W., Hsieh, J.C., Nakajima, S., Haussler, C.A., Whitfield, G.K. & Haussler, M.R. (1996) Human vitamin D receptor phosphorylation by casein kinase II at Ser-208 potentiates transcriptional activation. *Proc. Natl Acad. Sci. USA* **93**, 3519–3524.
13. Rochel, N., Wurtz, J.M., Mitschler, A., Klaholz, B. & Moras, D. (2000) The crystal structure of the nuclear receptor for vitamin D bound to its natural ligand. *Mol. Cell* **5**, 173–179.
14. Claire, M., Raffestin-Oblin, M.E., Michaud, A., Corvol, P., Venot, A., Roth-Meyer, C., Boisvieux, J.F. & Mallet, A. (1978) Statistical test of models and computerised parameter estimation for aldosterone binding in rat kidney. *FEBS Lett.* **88**, 295–299.
15. Zhao, X.Y., Eccleshall, T.R., Krishnan, A.V., Gross, C. & Felfman, D. (1997) Analysis of vitamin D analog-induced heterodimerization of vitamin D receptor with retinoid X receptor using the yeast two-hybrid system. *Mol. Endocrinol.* **11**, 366–378.
16. Birck, C., Vachette, P., Welch, M., Swaren, P. & Samama, J.P. (1996) Is the function of the cdc2 kinase subunit proteins tuned by their propensities to oligomerize? Conformational states in solution of the cdc2 kinase partners $p13^{suc1}$ and $p9^{cksphy}$. *Biochemistry* **35**, 5577–5585.
17. Xiao, J.H., Davidson, I., Matthes, H., Garnier, J.M. & Chambon, P. (1991) Cloning, expression and transcriptional properties of the human enhancer factor TEF-1. *Cell* **65**, 551–568.
18. Depautex, C., Desvignes, P., Leboucher, P., Lemonnier, M., Dagenaux, D., Benoit, J.P. & Vachette, P. (1987) *The Small Angle X-ray Scattering Instrument D24.* CNRS annual report LURE, Orsay, France.
19. Svergun, D., Barberato, C. & Koch, M.H.J. (1995) CRYSOL a program to evaluate X-ray solution scattering of biological macromolecules from atomic coordinates. *J. Appl. Cryst.* **28**, 768–773.
20. Svergun, D.I., Richard, S., Koch, M.H.J., Sayers, Z., Kuprin, S. & Zaccai, G. (1998) Protein hydration in solution: experimental observation by X-ray and neutron scattering. *Proc. Natl Acad. Sci. USA* **95**, 2267–2272.
21. Guinier, A. & Fournet, G. (1955) *Small Angle X-Ray Scattering.* Wiley, New York.
22. Glatter, O. & Kratky, O. (1982) *Small-Angle X-Ray Scattering.* Academic Press, New-York.
23. Svergun, D.I., Semenyuk, A.V. & Feigin, L.A. (1988) Small angle data scattering treatment by the regularization method. *Acta Crystallogr.* **A44**, 244–250.
24. Heidorn, D.B. & Trewhella, J. (1988) Comparison of the crystal and solution structures of calmodulin and troponin C. *Biochemistry* **27**, 909–915.
25. Nakajima, S., Hsieh, J.-C., MacDonal, P.N., Haussler, C.A., Galligan, M.A., Jurutka, P.W. & Haussler, M.R. (1993) Purified human vitamin D receptor overexpressed in *E. coli* and baculovirus systems does not bind 1,25-dihydroxyvitamin D_3 hormone efficiently unless supplemented with a rat liver nuclear extract. *Biochem. Biophys. Res. Comm.* **197**, 478–485.
26. Schaefer-Klein, J., Londowski, J.M. & Kumar, R. (1993) Bacterial synthesis of truncated forms of the human vitamin D receptor and characterization of anti-receptor monoclonal antibodies. *Biochem. Biophys. Res. Comm.* **196**, 167–172.
27. Craig, T.A. & Kumar, R. (1996) Synthesis and purification of soluble ligand binding domain of the human vitamin D_3 receptor. *Biochem. Biophys. Res. Comm.* **218**, 902–907.
28. Mottershead, D.G., Polly, P., Lyons, R.J., Sutherland, R.L. & Watts, C.K. (1996) High activity, soluble, bacterially expressed human vitamin D receptor and its ligand binding domain. *J. Cell Biochem.* **61**, 325–337.
29. Sone, T., McDonnell, D.P., O'Malley, B.W. & Pike, J.W. (1990) Expression of human vitamin D receptor in *Saccharomyces cervisiae*. *J. Biol. Chem.* **265**, 21997–22003.
30. MacDonald, P.N., Haussler, C.A., Terpening, C.M., Galligan, M.A., Reeder, M.C., Whitfied, G.K. & Haussler, M.R. (1991) Baculovirus-mediated expression of the human vitamin D receptor. *J. Biol. Chem.* **266**, 18808–18813.
31. Juntunen, K., Rochel, N., Moras, D. & Vihko, P. (1999) Large-scale expression and purification of the human vitamin D receptor and its ligand-binding domain for structural studies. *Biochem. J.* **344**, 297–303.
32. Väisänen, S., Juntunen, K., Itkonen, A., Vihko, P. & Mäenpää, P. (1997) Conformational studies of human vitamin-D receptor by antipeptide antibodies, partial proteolytic digestion and ligand binding. *Eur. J. Biochem.* **248**, 156–162.
33. Cheskis, B. & Freedman, L.P. (1996) Modulation of nuclear receptor interactions by ligands: kinetic analysis using surface plasmon resonance. *Biochemistry* **35**, 3309–3318.
34. Dong, D. & Noy, N. (1998) Heterodimer formation by retinoid X receptor: regulation by ligands and by the receptor's self association properties. *Biochemistry* **37**, 10691–10700.
35. Craig, T.A., Benson, L.M., Tomlinson, A.J., Veenstra, T.D., Naylor, S. & Kumar, R. (1999) Analysis of transcription complexes and effects of ligands by microelectrospray ionization mass spectrometry. *Nat. Biotech.* **17**, 1214–1218.
36. Luzzati, V. & Tardieu, A. (1980) Recent developments in solution X-ray scattering. *Ann. Rev. Biophys. Bioeng.* **9**, 1–29.
37. Trewhella, J. (1997) Insights into biomolecular structures function from small angle scattering. *Curr. Opin. Struct. Biol.* **7**, 702–708.
38. Michigami, T., Suga, A., Yamazaki, M., Shimizu, C., Cai, G., Okada, S. & Ozono, K. (1999) Identification of amino acid sequence in the hinge region of human vitamin D receptor that transfers a cytosolic protein to the nucleus. *J. Biol. Chem.* **274**, 33531–33538.